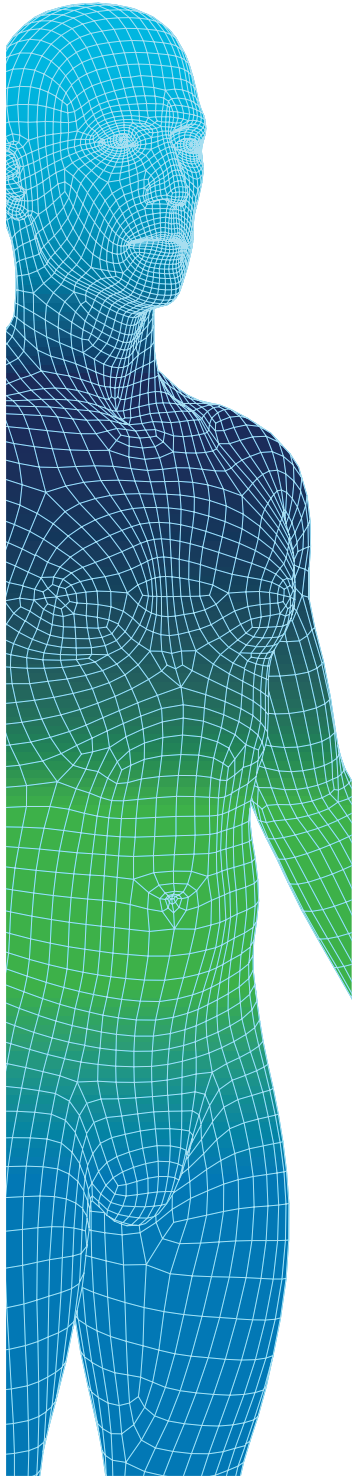

Dose Volume Histogram Limits

Conventional Fractionation

Structure Name	Type	Volume	Dose	Notes
Brachial plexus	Max Dose	None	<66 Gy	1
Brachial plexus	Volume (%)	5%	<60 Gy	1
Brainstem	Max Dose	None	<54 Gy	2
Brainstem	Volume (%)	1%	<60 Gy	2 (1% of PTV)
Cochlea	Volume (%)	5%	<55 Gy	3
Ears (inner/middle)	Mean Dose	None	<50 Gy	4
Eyes	Max Dose	None	<50 Gy	3
Eyes	Mean Dose	None	<35 Gy	4
Glottic larynx	Mean Dose	None	<45 Gy	4
Lens	Max Dose	None	<25 Gy	5
Mandible	Max Dose	None	<70 Gy	2
Mandible	Volume (cc)	<1cc	75 Gy	2
Optic nerves	Max Dose	None	<54 Gy	2
Optic nerves	Volume (%)	1%	<60 Gy	2 (1% of PTV)
Oral cavity	Mean Dose	None	<40 Gy	3 (excluding PTV)
Parotid gland (one)	Mean Dose	None	<26 Gy	6 (if sparing one)
Parotid gland (one)	Volume (%)	50%	<30 Gy	6 (if sparing one)
Parotid gland (both)	Volume (cc)	<20cc	20 Gy	6 (if sparing both)
Temporal lobes	Max Dose	None	<60 Gy	2
Temporal lobes	Volume (%)	1%	<65 Gy	2 (1% of PTV)
T-M joint	Max Dose	None	<70 Gy	2
T-M joint	Volume (cc)	<1cc	75 Gy	2
Tongue	Max Dose	None	<55 Gy	2
Tongue	Volume (%)	1%	<65 Gy	2 (1% of PTV)
Esophagus	Mean Dose	None	<35 Gy	7 (45 Gy if necessary)
Esophagus	Volume (%)	15%	<54 Gy	7 (65 Gy if necessary)
Esophagus	Volume (%)	33%	<45 Gy	7 (50 Gy if necessary)
Heart	Volume (%)	33%	<60 Gy	8
Heart	Volume (%)	67%	<45 Gy	8
Heart	Volume (%)	100%	<40 Gy	8
Lung (right and left)	Mean Dose	None	<20 Gy	9 (lung minus GTV)
Lung (right and left)	Volume (%)	37%	<20 Gy	9 (lung minus GTV)
Pharyngeal constrictor	Mean Dose	None	<54 Gy	10
Pharyngeal constrictor	Volume (%)	51%	<50 Gy	10
Pharyngeal constrictor	Volume (%)	60%	<52 Gy	10
Duodenum	Max Dose	None	<60 Gy	11
Duodenum	Volume (%)	33%	<45 Gy	11
Kidney	Volume (%)	33%	<50 Gy	12
Kidney	Volume (%)	67%	<30 Gy	12
Kidney	Volume (%)	100%	<23 Gy	12
Liver	Volume (%)	50%	<35 Gy	13
Liver	Volume (%)	100%	<30 Gy	13
Small intestine	Max Dose	None	<50 Gy	14
Small intestine	Volume (cc)	<100cc	40 Gy	14
Small intestine	Volume (cc)	<180cc	35 Gy	14
Small intestine	Volume (cc)	<65cc	45 Gy	14
Stomach	Max Dose	None	<54 Gy	11
Stomach	Volume (%)	2%	<50 Gy	11
Stomach	Volume (%)	25%	<45 Gy	11
Bladder	Volume (%)	15%	<80 Gy	15
Bladder	Volume (%)	25%	<75 Gy	15
Bladder	Volume (%)	35%	<70 Gy	15
Bladder	Volume (%)	50%	<65 Gy	15
Femoral heads	Max Dose	None	<50 Gy	14
Femoral heads	Volume (%)	25%	<45 Gy	14
Femoral heads	Volume (%)	40%	<40 Gy	14
Penile bulb	Mean Dose	None	<52.5 Gy	15
Rectum	Volume (%)	15%	<75 Gy	15
Rectum	Volume (%)	25%	<70 Gy	15
Rectum	Volume (%)	35%	<65 Gy	15
Rectum	Volume (%)	50%	<60 Gy	15
Spinal cord	Max Dose	None	<45 Gy	16

1 Fraction SRS

Structure Name	Type	Volume	Dose	Notes
Brachial plexus	Max Dose	None	<17.5 Gy	17
Brachial plexus	Volume (cc)	<3cc	14 Gy	17
Brain	Volume (cc)	<10cc	10 Gy	18
Brainstem	Max Dose	None	<15 Gy	19
Brainstem	Volume (cc)	<0.5cc	10 Gy	19
Cochlea	Max Dose	None	<9 Gy	20
Optic nerves	Max Dose	None	<10 Gy	21
Optic nerves	Volume (cc)	<0.2cc	8 Gy	21
Bronchus	Max Dose	None	<13.3 Gy	22
Bronchus	Volume (cc)	<0.5cc	12.4 Gy	22
Esophagus	Max Dose	None	<15.4 Gy	23
Esophagus	Volume (cc)	<5cc	11.9 Gy	23
Great vessels	Max Dose	None	<37 Gy	24
Great vessels	Volume (cc)	<10cc	31 Gy	24
Heart	Max Dose	None	<22 Gy	25
Heart	Volume (cc)	<15cc	16 Gy	25
Lung (right and left)	Vol. to Spare	>1000cc	7.4 Gy	26
Lung (right and left)	Vol. to Spare	>1500cc	7 Gy	27
Rib	Max Dose	None	<30 Gy	28
Rib	Volume (cc)	<1cc	22 Gy	28
Trachea	Max Dose	None	<20.2 Gy	23
Trachea	Volume (cc)	<4cc	10.5 Gy	23
Colon	Max Dose	None	<18.4 Gy	29
Colon	Volume (cc)	<20cc	14.3 Gy	29
Duodenum	Max Dose	None	<12.4 Gy	30
Duodenum	Volume (cc)	<10cc	9 Gy	30
Duodenum	Volume (cc)	<5cc	11.2 Gy	30
Jejunum/ileum	Max Dose	None	<15.4 Gy	31
Jejunum/ileum	Volume (cc)	<5cc	11.9 Gy	31
Liver	Vol. to Spare	>700cc	9.1 Gy	32
Renal cortex (right and left)	Vol. to Spare	>200cc	8.4 Gy	33
Renal hilum/ vascular trunk	Volume (%)	66%	<10.6 Gy	34
Stomach	Max Dose	None	<12.4 Gy	35
Stomach	Volume (cc)	<10cc	11.2 Gy	35
Bladder wall	Max Dose	None	<18.4 Gy	36
Bladder wall	Volume (cc)	<15cc	11.4 Gy	36
Cauda equina	Max Dose	None	<16 Gy	21
Cauda equina	Volume (cc)	<5cc	14 Gy	21
Femoral heads	Volume (cc)	<10cc	14 Gy	37
Penile bulb	Max Dose	None	<34 Gy	38
Penile bulb	Volume (cc)	<3cc	14 Gy	38
Rectum	Max Dose	None	<18.4 Gy	39
Rectum	Volume (cc)	<20cc	14.3 Gy	39
Sacral plexus	Max Dose	None	<16 Gy	17
Sacral plexus	Volume (cc)	<5cc	14.4 Gy	17
Skin	Max Dose	None	<26 Gy	30
Skin	Volume (cc)	<10cc	23 Gy	30
Spinal cord	Max Dose	None	<14 Gy	40
Spinal cord	Volume (cc)	<0.35cc	10 Gy	40
Spinal cord	Volume (cc)	<1.2cc	7 Gy	40

3 Fraction SBRT

Structure Name	Type	Volume	Dose	Notes
Brachial plexus	Max Dose	None	<24 Gy	17
Brachial plexus	Volume (cc)	<3cc	20.4 Gy	17
Brainstem	Max Dose	None	<23.1 Gy	19
Brainstem	Volume (cc)	<0.5cc	18 Gy	19
Cochlea	Max Dose	None	<17.1 Gy	20
Optic nerves	Max Dose	None	<17.4 Gy	21
Optic nerves	Volume (cc)	<0.2cc	15.3 Gy	21
Bronchus	Max Dose	None	<23.1 Gy	22
Bronchus	Volume (cc)	<0.5cc	18.9 Gy	22
Esophagus	Max Dose	None	<25.2 Gy	23
Esophagus	Volume (cc)	<5cc	17.7 Gy	23
Great vessels	Max Dose	None	<45 Gy	24
Great vessels	Volume (cc)	<10cc	39 Gy	24
Heart	Max Dose	None	<30 Gy	25
Heart	Volume (cc)	<15cc	24 Gy	25
Lung (right and left)	Vol. to Spare	>1000cc	12.4 Gy	26
Lung (right and left)	Vol. to Spare	>1500cc	11.6 Gy	27
Rib	Max Dose	None	<36.9 Gy	28
Rib	Volume (cc)	<1cc	28.8 Gy	28
Rib	Volume (cc)	<30cc	30 Gy	28
Trachea	Max Dose	None	<30 Gy	23
Trachea	Volume (cc)	<4cc	15 Gy	23
Colon	Max Dose	None	<28.2 Gy	29
Colon	Volume (cc)	<20cc	24 Gy	29
Duodenum	Max Dose	None	<22.2 Gy	30
Duodenum	Volume (cc)	<10cc	11.4 Gy	30
Duodenum	Volume (cc)	<5cc	16.5 Gy	30
Jejunum/ileum	Max Dose	None	<25.2 Gy	31
Jejunum/ileum	Volume (cc)	<5cc	17.7 Gy	31
Liver	Vol. to Spare	>700cc	19.2 Gy	32
Renal cortex (right and left)	Vol. to Spare	>200cc	16 Gy	33
Renal hilum/ vascular trunk	Volume (%)	66%	<18.6 Gy	34
Stomach	Max Dose	None	<22.2 Gy	35
Stomach	Volume (cc)	<10cc	16.5 Gy	35
Bladder wall	Max Dose	None	<28.2 Gy	36
Bladder wall	Volume (cc)	<15cc	16.8 Gy	36
Cauda equina	Max Dose	None	<24 Gy	21
Cauda equina	Volume (cc)	<5cc	21.9 Gy	21
Femoral heads	Volume (cc)	<10cc	21.9 Gy	37
Penile bulb	Max Dose	None	<42 Gy	38
Penile bulb	Volume (cc)	<3cc	21.9 Gy	38
Rectum	Max Dose	None	<28.2 Gy	39
Rectum	Volume (cc)	<20cc	24 Gy	39
Sacral plexus	Max Dose	None	<24 Gy	17
Sacral plexus	Volume (cc)	<5cc	22.5 Gy	17
Skin	Max Dose	None	<33 Gy	30
Skin	Volume (cc)	<10cc	30 Gy	30
Spinal cord	Max Dose	None	<21.9 Gy	40
Spinal cord	Volume (cc)	<0.35cc	18 Gy	40
Spinal cord	Volume (cc)	<1.2cc	12.3 Gy	40

5 Fraction SBRT

Structure Name	Type	Volume	Dose	Notes
Brachial plexus	Max Dose	None	<30.5 Gy	17
Brachial plexus	Volume (cc)	<3cc	27 Gy	17
Brainstem	Max Dose	None	<31 Gy	19
Brainstem	Volume (cc)	<0.5cc	23 Gy	19
Cochlea	Max Dose	None	<25 Gy	20
Optic nerves	Max Dose	None	<25 Gy	21
Optic nerves	Volume (cc)	<0.2cc	23 Gy	21
Bronchus	Max Dose	None	<33 Gy	22
Bronchus	Volume (cc)	<0.5cc	21 Gy	22
Esophagus	Max Dose	None	<35 Gy	23
Esophagus	Volume (cc)	<5cc	19.5 Gy	23
Great vessels	Max Dose	None	<53 Gy	24
Great vessels	Volume (cc)	<10cc	47 Gy	24
Heart	Max Dose	None	<38 Gy	25
Heart	Volume (cc)	<15cc	32 Gy	25
Lung (right and left)	Vol. to Spare	>1000cc	13.5 Gy	26
Lung (right and left)	Vol. to Spare	>1500cc	12.5 Gy	27
Rib	Max Dose	None	<43 Gy	28
Rib	Volume (cc)	<1cc	35 Gy	28
Trachea	Max Dose	None	<40 Gy	23
Trachea	Volume (cc)	<4cc	16.5 Gy	23
Colon	Max Dose	None	<38 Gy	29
Colon	Volume (cc)	<20cc	25 Gy	29
Duodenum	Max Dose	None	<32 Gy	30
Duodenum	Volume (cc)	<10cc	12.5 Gy	30
Duodenum	Volume (cc)	<5cc	18 Gy	30
Jejunum/ileum	Max Dose	None	<35 Gy	31
Jejunum/ileum	Volume (cc)	<5cc	19.5 Gy	31
Liver	Vol. to Spare	>700cc	21 Gy	32
Renal cortex (right and left)	Vol. to Spare	>200cc	17.5 Gy	33
Renal hilum/ vascular trunk	Volume (%)	66%	<23 Gy	34
Stomach	Max Dose	None	<32 Gy	35
Stomach	Volume (cc)	<10cc	18 Gy	35
Bladder wall	Max Dose	None	<38 Gy	36
Bladder wall	Volume (cc)	<15cc	18.3 Gy	36
Cauda equina	Max Dose	None	<32 Gy	21
Cauda equina	Volume (cc)	<5cc	30 Gy	21
Femoral heads	Volume (cc)	<10cc	30 Gy	37
Penile bulb	Max Dose	None	<50 Gy	38
Penile bulb	Volume (cc)	<3cc	30 Gy	38
Rectum	Max Dose	None	<38 Gy	39
Rectum	Volume (cc)	<20cc	25 Gy	39
Sacral plexus	Max Dose	None	<32 Gy	17
Sacral plexus	Volume (cc)	<5cc	30 Gy	17
Skin	Max Dose	None	<39.5 Gy	30
Skin	Volume (cc)	<10cc	36.5 Gy	30
Spinal cord	Max Dose	None	<30 Gy	40
Spinal cord	Volume (cc)	<0.35cc	23 Gy	40
Spinal cord	Volume (cc)	<1.2cc	14.5 Gy	40

Notes and Sources

1: RTOG 0619
2: RTOG 0225, use either max dose or volume
3: RTOG 0615
4: RTOG 0225
5: RTOG 0615, cataracts
6: RTOG 0912, xerostomia
7: RTOG 0920
8: RTOG 0623
9: RTOG 0623, clinical pneumonitis
10: Caglar et al., IJROBP 72, 1110-1118 (2008)
11: Spalding et al., Med Phys 34, 521-529 (2007)
12: RTOG 0436, renal insufficiency
13: RTOG 0436, clinical hepatitis
14: RTOG 0822
15: RTOG 0126
16: RTOG 0623, myelitis
17: TG-101, neuropathy
18: Chin et al., J Neurosurg 94, 899-904 (2001)
19: TG-101, cranial neuropathy
20: TG-101, hearing loss
21: TG-101, neuritis
22: TG-101, stenosis with atelectasis
23: TG-101, stenosis/fistula
24: TG-101, aneurysm
25: TG-101, pericarditis
26: TG-101, pneumonitis
27: TG-101, basic lung function
28: TG-101, pain or fracture
29: TG-101, colitis/fistula
30: TG-101, ulceration
31: TG-101, enteritis/obstruction
32: TG-101, basic liver function
33: TG-101, basic renal function
34: TG-101, malignant hypertension
35: TG-101, ulceration/fistula
36: TG-101, cystitis/fistula
37: TG-101, necrosis
38: TG-101, impotence
39: TG-101, proctitis/fistula
40: TG-101, myelitis

Mobius3D

Mobius3D software automatically checks DVH limits for your plans, making this chart a thing of the past.

MOBIUS MEDICAL SYSTEMS

Mobius Medical Systems provides the radiation oncology community with modern software to improve productivity of quality assurance processes and increase positive patient outcomes.
Visit www.mobiusmed.com for more information.

Original Article

PMP

Progress in Medical Physics 30(1), March 2019
https://doi.org/10.14316/pmp.2019.30.1.22
eISSN 2508-4453

b0 Dependent Neuronal Activation in the Diffusion-Based Functional MRI

Hyug-Gi Kim[1], Geon-Ho Jahng[2]

[1]Department of Biomedical Engineering, Graduate School, Kyung Hee University, Yongin, [2]Department of Radiology, Kyung Hee University Hospital at Gangdong, College of Medicine, Kyung Hee University, Seoul, Korea

Received 14 January 2019
Revised 5 March 2019
Accepted 5 March 2019

Corresponding author
Geon-Ho Jahng
(ghjahng@gmail.com)
Tel: 82-2-440-6187
Fax: 82-2-440-6932

Purpose: To develop a new diffusion-based functional MRI (fMRI) sequence to generate apparent diffusion coefficient (ADC) maps in single excitation and evaluate the contribution of b0 signal on neuronal changes.

Materials and Methods: A diffusion-based fMRI sequence was designed with single measurement that can acquire images of three directions at a time, obtaining b = 0 s/mm^2 during the first baseline condition (b0_b), followed by 107 diffusion-weighted imaging (DWI) with b = 600 s/mm^2 during the baseline and visual stimulation conditions, and another b = 0 s/mm^2 during the last activation condition (b0_a). ADC was mapped in three different ways: 1) using b0_b (ADC_b) for all time points, 2) using b0_a (ADC_a) for all time points, and 3) using b0_b and b0_a (ADC_ba) for baseline and stimulation scans, respectively. The fMRI studies were conducted on the brains of 16 young healthy volunteers using visual stimulations in a 3T MRI system. In addition, the blood oxygen level dependent (BOLD) fMRI was also acquired to compare it with diffusion-based fMRI. A sample t-test was used to investigate the voxel-wise average between the subjects.

Results: The BOLD data consisted of only activated voxels. However, ADC_ba data was observed in both deactivated and activated voxels. There were no statistically significant activated or deactivated voxels for DWI, ADC_b, and ADC_a.

Conclusions: With the new sequence, neuronal activations can be mapped with visual stimulation as compared to the baseline condition in several areas in the brain. We showed that ADC should be mapped using both DWI and b0 images acquired with the same conditions.

Keywords: Brain function, Functional MRI, Diffusion, ADC, BOLD

Introduction

Functional MRI (fMRI) has the ability to detect local signal increase secondary to behavioral tasks, has provided a powerful tool for cognitive neurosciences, and offers noninvasive access to the cortical and subcortical neuronal functions.[1)] fMRI relies on the common principle that regional blood flow and metabolism are modulated by neuronal activity.[2)] The blood oxygen level-dependent (BOLD) contrast is most common approach.[3-5)] During a brain stimulation, oxygen consumption increases and thus the blood flow increases largely, resulting in a net decrease of the blood deoxyhemoglobin concentration, which, in turn, leads to a measurable signal increase because deoxyhemoglobin is paramagnetic.[1)]

Diffusion MRI provides quantitative data on water molecular motion which is a very sensitive marker of tissue microstructures.[6)] The random displacements of water molecules provide valuable information on the cell size or cell orientation in tissues.[7)] MRI is only the means to

observe in vivo diffusion, noninvasively. The diffusion-weighted imaging (DWI) signals are measured with and without applying diffusion gradients to map voxel-based apparent diffusion coefficient (ADC). DWI is routinely used in patients with brain strokes or tumors. Signal increase in DWI reflects a decrease of the ADC of water which has been ascribed to a phase transition of a fraction of water molecules from a fast to a slower diffusion pool in the pathological areas[8,9] or cortex undergoing activation.[10] In addition, diffusion-based fMRI was applied to measure neuronal responses after some tasks.[6,10] The advantage of diffusion-based fMRI is that the signal contribution of blood itself can be reduced by the applied diffusion gradients, means that fMRI signal originates from neuronal tissues rather than blood vascular.

To calculate the ADC value from DWI, the signal, which is acquired without diffusion gradient and is called as b0, is used. The b0 signal may be affected on the signal alternations of diffusion-based fMRI experiments. Therefore, the purpose of this study was to develop a new diffusion-based fMRI sequence to generate ADC maps in a single excitation and to evaluate the b0 signal contribution on the neuronal changes.

Materials and Methods

1. Pulse sequence design

A diffusion-weighted spin-echo pulse sequence has a pair of diffusion gradients around the refocusing pulse. As mentioned before, DWI should be acquired at least twice with (b-value) and without (b0) applying diffusion gradients. Furthermore, to obtain an isotropic ADC value, DWI signals should be acquired with minimum three directions, which are slice-selection, phase-encoding, and frequency-encoding directions. Therefore, we have to scan at least four times to map isotropic diffusion. For the fMRI study, this scan must be repeated to several times with and without stimulations to map neuronal changes. This takes a long scan times so it is not suitable for fMRI and a subject can be moved during scans. Therefore, we developed a new sequence to minimize the scan time during diffusion-based fMRI by two approaches.

First, the diffusion-based fMRI sequence was designed with a single measurement. Therefore, the sequence was designed to acquire a single DWI with applying diffusion gradients in three directions at a time (Fig. 1a).[11] To develop the sequence, the pulsed-gradient spin-echo (PGSE) pulse sequence was based.[12] For DWI, the diffusion gradients were applied around the refocusing pulse on the three axes, but shifted in each axis that the diffusion gradient was not applied simultaneously. The diffusion gradient on the phase-encoding axis (G_y) was started after applying the first diffusion gradient on the readout-encoding axis (G_x). The diffusion gradient on the slice-selective axis was also started after applying the first diffusion gradient on the phase-encoding axis (G_z). In this way, three diffusion gradients do not interact with the diffusion pairs. The duration of the applied diffusion gradient in each axis was shorter than those applied on the general PGSE diffusion gradient. The diffusion weighting factor b is given by

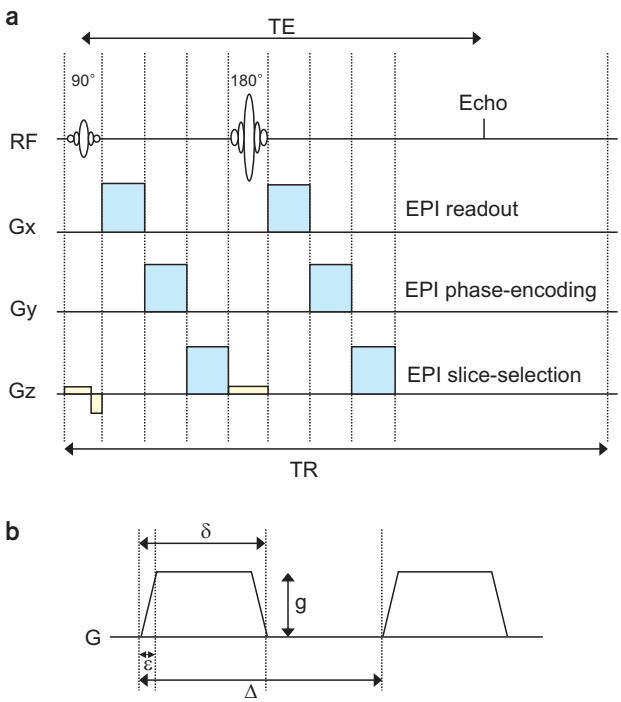

Fig. 1. Diagrams of the diffusion-based functional MRI sequence (a) and the gradient for diffusion-weighting (b). Diffusion gradients were applied on the three axes to map isotropic apparent diffusion coefficient in a single acquisition. (a) RF, radio frequency; Gx, readout direction; Gy, phase-encoding direction; Gz, slice-selection direction; TE, echo time; TR, repetition time; and Echo, echo signal. (b) g, gradient strength; δ, duration of the diffusion gradient; ε, length of slope (ramp time); Δ, diffusion time.

$$b=\gamma^2 g^2 \left[\delta^2\left(\Delta-\frac{\delta}{3}\right)+\frac{\varepsilon^3}{30}-\frac{8\varepsilon^2}{6}\right] \quad (1)$$

in which γ is the gyromagnetic ratio, g is the gradient strength and δ is the duration of the diffusion gradient, ε is length of slope (ramp time), and Δ is the diffusion time. In our experiments (Fig. 1b), δ was set to 8.27 ms, Δ was 35 ms, ε was 0.98 ms and the maximum gradient strengths were was 35.6 mT/m for both G_x and G_y and –35.6 mT/m for G_z. Diffusion gradients were applied along three orthogonal axes simultaneously (i.e., $b=b_x+b_y+b_z$ with $|b_x|=|b_y|=|b_z|$). The b-factor for each axis was 200 s/mm^2.

Second, b0 images, which were acquired without applying diffusion gradient, were acquired to twice to quantify the ADC map for each DWI scan (Fig. 2a). The ADC map can be calculated by combining at least two DWIs that are differently sensitized to diffusion, but remain identical with respect to the other parameters, for instance, the image S_0 without diffusion weighting (b=0 s/mm^2) and one DWI (b> 0 s/mm^2). We calculated an ADC value for each pixel with the following equation,

$$ADC_i = -\frac{1}{b}\ln\left(\frac{S_i}{S_0}\right) \quad (2)$$

where S_o and S_i were the signal intensities in a given voxel without (b0) and with applying the diffusion sensitization gradient at the time *i* respectively. Therefore, to map ADC, DWI with certain b-value and b=0 should be always acquired. However, it is inefficient and it needs long scan time to scan S0 image every time point with DWI. Therefore, the diffusion-based fMRI sequence was designed to scan optimally (Fig. 2a). One DWI with b=0 s/mm^2 was obtained during the first baseline scan (b0_b) and then 107 DWIs with b=600 s/mm^2 were imaged with altering the baseline and stimulation conditions. Finally, another DWI with b=0 s/mm^2 was again obtained during the last stimulation scan (b0_a). Therefore, two b0 images were scanned with the baseline and activation conditions, separately. ADCs were mapped with three different ways: 1) using b0_b (ADC_b) for all 107 time points, 2) using b0_a (ADC_a) for all 107 time points, and 3) using both b0_b for the baseline DWI scans and b0_a for the stimulation DWI scans (ADC_ba) . Therefore, we had diffusion-based fMRI data for DWI which was the original dynamic diffusion-weighted serial images, ADC_b serial images, ADC_a serial images, and ADC_ba serial images. The diffusion-based fMRI sequence was implemented in the Philips pulse programming environment (Rel ver 3.6.0).

2. Subjects

Sixteen healthy volunteers (7 males, 9 females) were recruited from the local community. None of the volunteers had neurological or psychiatry disease history. All young controls underwent Korean Version of Mini-Mental State Examination (K-MMSE) test based on global cognitive ability and brain fMRI scans. One of the subjects had too many motion-related artifacts and therefore fifteen subjects were finally included in this study. Mean ages were 26.4±2.6 years (range: 20 to 30 years). Mean K-MMSE scores were 29.7±0.7 (The maximum score is 30). This study was performed with approval of the local institution review board

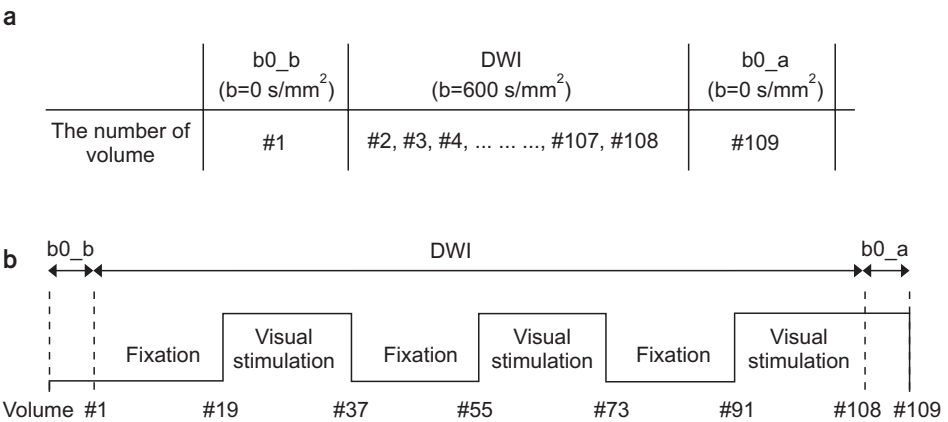

Fig. 2. The scan orders (a) and the stimulation paradigm (b) for the diffusion-based functional MRI acquisitions. The same stimulation paradigm was applied on the BOLD fMRI scans.
b0_b, the first baseline scan; b0_a, the last activation scan; DWI, diffusion-weighted imaging scans.

and all subjects were provided prior written consent.

3. Functional MRI paradigm

In this study, two functional sessions, which were BOLD fMRI and DWI-based fMRI, were performed from each subject. The paradigm for visual stimulation was used for two conditions which had a fixation for the baseline condition and a black-and-white checkerboard for the stimulation condition (Fig. 2b). A cross-sign was used for the fixation condition. This alternation was repeated three times for each session. The duration of each block was 63 sec for the diffusion-based fMRI and 54 sec for BOLD fMRI. Number of scans per each block was 18 for both diffusion-based fMRI and BOLD fMRI. There were 109 and 108 dynamic volumes for the diffusion-based fMRI and BOLD fMRI, respectively. The stimulation paradigm was presented using the Esys fMRI Manager Client system (Invivo, Orlando, FL, USA).

4. MR data acquisitions

MR imaging was performed on a 3 Tesla MRI System (Achieva, Philips Medical System, Best, The Netherlands) with an 8 channel phase-array sensitivity-encoding (SENSE) coil. The diffusion-based fMRI data were acquired with our sequence with the following parameters: repetition time (TR)=3500 ms, TE=70.41 ms, field of view (FOV)=230×230×120 mm, matrix size=64×49 mm, voxel size= 2.4×2.4×6 mm^3, slices = 42, SENSE factor=2, and flip angle=90°. The max b-factor was 600 s/mm^2. The scan time was 6 min 28 sec.

To compare brain activations with the diffusion-based fMRI, BOLD fMRI data were also acquired using a gradient-echo echo-planar imaging (EPI) sequence with the following parameters: TR=3000 ms, TE=30 ms, FOV=230×120×230 mm, matrix size=64×64 mm, voxel size=2.4×2.4×6 mm^3, direction = axial, slice thickness = 6 mm without gap, slices=20, SENSE factor=2, and flip angle=90°. The scan time was 5 min 45 sec.

In addition, volumetric three-dimensional T1-weighted images (3D T1WI) were acquired with the magnetization prepared rapid acquisition gradient-echo (MPRGE) sequence for the fMRI processing step with the following parameters: TR=8.2 ms, TE = 3.8 ms, inversion time (TI)=1022 ms, flip angle=8°, SENSE factor=2.5, FOV=236×236×170 mm, matrix size=236×236 mm, slice thickness=1 mm, voxel size=1×1×1 mm^3, and the number of slice=340.

5. Data processing

Statistical parametric mapping version 5 (SPM5) (Wellcome Department of Imaging Neuroscience, University College London, UK) software was used for data preprocessing and statistical analysis. First of all, the functional images of each subject were realigned to the first volume to minimize the effect of head motion during the brain scan and were created the mean image. And then, the functional mean image was co-registered to the corresponding structural 3D T1WI. After that, 3D T1WI and the corresponding fMRI data were spatially normalized onto the standard Montreal Neurological Institute (MNI) template by using the non-linear transformations.[13] The functional images were then smoothed with full width at half maximum (FWHM) of Gaussian Kernel of 8×8×10 mm.

6. Statistical tests

For the individual level (1st level) analysis, the activation or deactivation with the visual stimulation compared with the baseline condition for each subject was calculated for each session by a general linear model (GLM) approach[14] based on a voxel-by-voxel calculation. Therefore, there were two contrast maps, activation or deactivation for each session of the diffusion-based fMRI or BOLD fMRI data.

For the group level (2nd level) analysis, the two contrast maps obtained from the individual level analysis were used to investigate average of all subjects between stimulation and baseline conditions with using one-sample t-test. For all fMRI data, the activated or deactivated map during the visual stimulation against the baseline condition was identified with $P<0.001$ with corrected for multiple comparisons using a false discovery rate (FDR) and the extent threshold was 10 voxels. To find anatomical areas of the brain, the t-test results were standardized into Talairach coordinate[15] by using the GingerALE and the Talairach Client (University

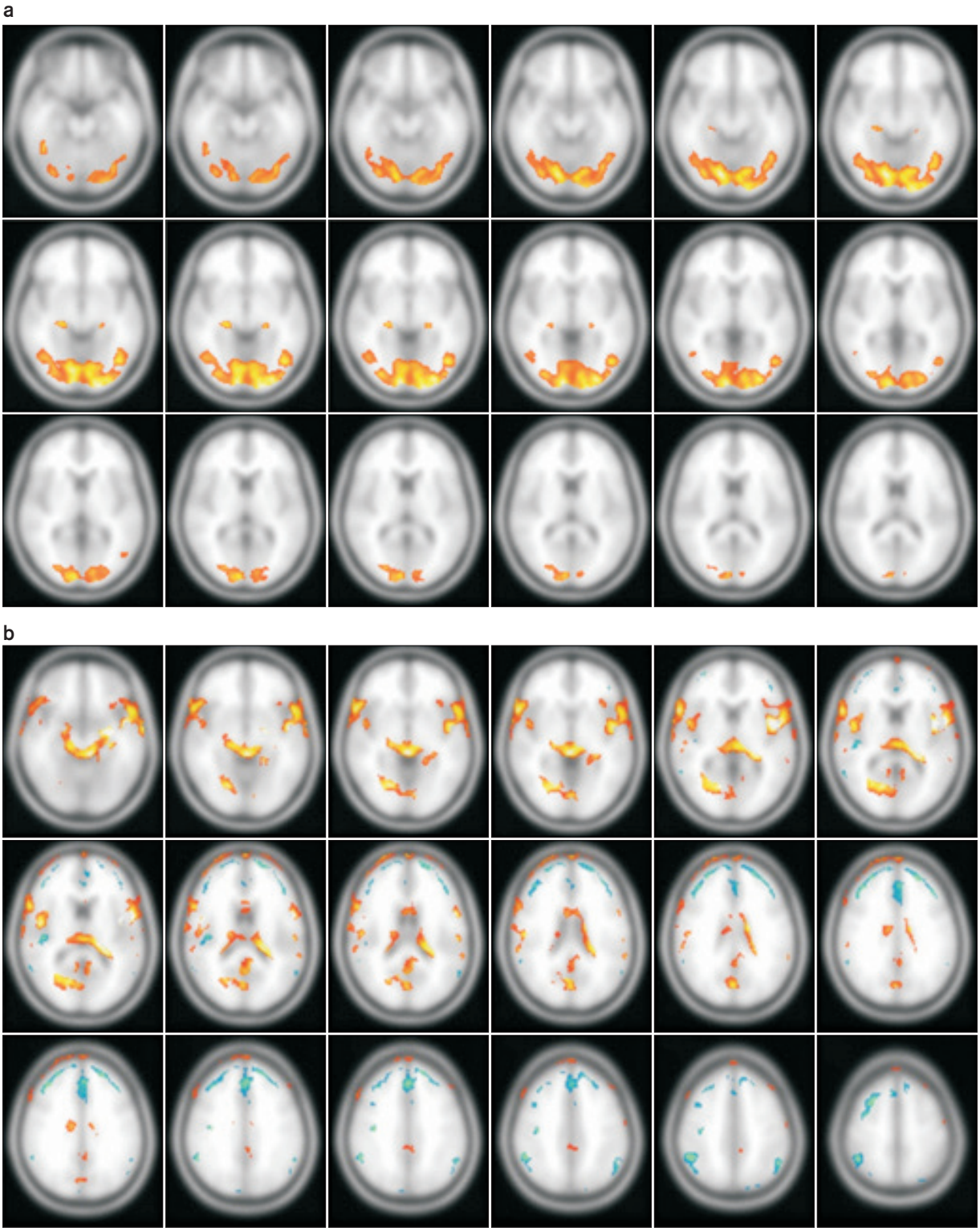

Fig. 3. Results of BOLD (a) and ADC_ba (b) for activated and deactivated brain regions for visual stimulation over 15 subjects. The results for activation and deactivation are observed with $P<0.001$ for correcting multiple comparisons using a false discovery rate (FDR), respectively. In the blood oxygen level-dependent (BOLD) data, increased (red) neuronal activations were found during the visual stimulation, and no deactivation areas were observed. In the ADC_ba data, increased (red) and decreased (blue) neuronal activations were found during the visual stimulation. ADC_ba was apparent diffusion coefficient (ADC) mapped with using both b0_b and b0_a for the baseline scans and activation scans, respectively. The color-coded maps are overlaid on the standard axial T1 template.

of Texas Health Science Center San Antonio, UTHSCSA) software.

Results

Fig. 3 shows the results of the voxel-based group analysis for 15 subjects using the one sample t-test for BOLD (Fig. 3a) and ADC_ba (Fig. 3b) data. Deactivated or activated areas during visual stimulation are overlaid on the standard axial T1 template and are shown with red or blue colors, respectively. The BOLD data had only activated voxels without any deactivated voxels. A strong activation was shown in the occipital lobe. However, ADC_ba data were observed both deactivated and activated voxels and activation areas were spread in several brain areas. There were no statistically significantly activated or deactivated voxels for DWI, ADC_b, and ADC_a.

In the BOLD data, BOLD signals were increased with the visual stimulation condition compared to the baseline condition, mainly in the right lingual gyrus and the left inferior temporal gyrus in the occipital lobe. The detailed results are summarized in Table 1. In the ADC_ba data, neuronal activations were increased or decreased with the visual stimulation condition compared to the baseline condition. The increased activation areas were in the right lingual gyrus of the occipital lobe which was the same area with the BOLD fMRI data. The Z-score was similar to that with the BOLD fMRI result. Additional increased areas were observed in the frontal lobe, the parietal lobe, the temporal lobe, the limbic lobe. With the ADC_ba data, we also found in deactivated areas in the occipital lobe, the frontal lobe, the parietal lobe, and the temporal lobe. The detailed results are listed in Table 2.

Discussion

1. Important to select the b0 scan to map ADCseries for each condition

Result of the diffusion-based fMRI showed that neuronal activation depended on the b0 signal. In this experiment, we acquired two different b0 images: one during the baseline condition and another during the stimulation condition. ADC maps were obtained with DWI with b=600 s/mm^2 using S0 acquired during the baseline condition, using S0 acquired during the stimulation condition, or using S0 acquired during both conditions. Our result showed that ADC mapped using both DWI and b0 images acquired with the same condition had high sensitive to map neuronal activations. Previous diffusion-based fMRI studies were not taken account into this issue.[1,6,10] If the stimulation condition between the b0 and DWI scans does not match, then neuronal activation can be minimized.

There are several published papers to study BOLD, diffusion-weighted, and ADC-fMRI.[16,17] Previous published studies were conducted as a stimulation of the visual system using a general diffusion gradient based sequence paradigm. The sequence, we developed, can be used to DWI scans with a relatively low b-value because of using the bipolar gradient for each axis. It may be problem to use it in the clinical applications such as strokes and tumors because it may be not sensitive to detect small lesions. However, in the fMRI study, we do not need to use a high b-value because only the vascular signal elimination

Table 1. Significantly activated brain regions during the visual stimulation using the blood oxygen level-dependent (BOLD) method in all subjects.

Region			BA	Talairach coordinate			Z-score	Cluster size
				X	Y	Z		
Activation (Stimulation " >" Baseline)								
Occipital lobe	Right	Lingual gyrus	18	8.04	−87.35	−5.66	6.46	8711
	Left	Inferior temporal gyrus	17	−15.99	−90.6	−9.98	6.43	8711
Sub-lobar	Right	Lateral geniculum		23.05	−25.59	−3.16	5.57	136
	Left	Lateral geniculum		−19.55	−27.41	−2.25	5.22	86

Results of one-sample t-test with P<0.005, correcting for multiple comparisons using a false discovery rate (FDR) and the extent threshold with 10 voxels. There were no deactivation (Visual stimulation <Baseline) areas.
BA, Brodmann area.

Table 2. Significantly activated or deactivated brain regions during the visual stimulation for ADC_ba data in all subjects.

Region			BA	Talairach coordinate			Z-score	Cluster size
				X	Y	Z		
Activation (Stimulation " >" Baseline)								
Occipital lobe	Right	Lingual gyrus	*	13.58	−65.54	1.9	6.47	1427
			19	17.39	−66.55	−7.14	6.4	1427
			19	24.74	−68.8	−3.62	5.93	1427
Frontal lobe	Right	Precentral gyrus	44	54.52	12.68	8.2	6.54	2405
		Superior frontal gyrus	9	19.17	59.04	35.42	5.05	509
				24.85	61.74	26.76	4.99	509
		Inferior frontal gyrus	47	23.45	13.94	−22.83	4.15	17
		Superior frontal gyrus	8	4.01	40.08	56.79	3.78	15
	Left	Precentral gyrus	6	−51.1	1.35	12.55	Inf	3084
		Superior frontal gyrus	10	0.77	63.56	28.33	5.52	509
			10	−34.35	54.95	21.51	4.38	57
		Middle frontal gyrus	10	−25.1	62.18	24.16	4.28	57
		Superior frontal gyrus	9	−17.82	59.4	33.03	3.86	57
			8	−38.53	22.19	48.97	4.23	41
		Precentral gyrus	4	−57.09	−16.49	41.39	4.02	25
		Superior frontal gyrus	6	−3.42	38.08	58.28	3.85	15
Parietal lobe	Left	Postcentral gyrus	40	−53.11	−23.56	17.36	5.58	40
			3	−49.8	−13.67	50.79	3.97	25
Temporal lobe	Left	Superior temporal gyrus	13	−56.9	−40.66	19.28	5.18	52
		Middle temporal gyrus	22	−54.83	−37.24	3.43	4.1	52
		Superior temporal gyrus	13	−43.42	1.54	−8.92	7.12	3084
Limbic lobe	Right	Posterior cingulate	30	6.11	−55.02	9.98	5.07	482
	Left	Parahippocampal gyrus, amygdala		−28.59	−7.51	−13.13	7.73	4307
		Posterior cingulate	29	−6.86	−51.4	11.9	5.37	482
			23	−1.35	−57.19	13.25	5.06	482
		Anterior cingulate	33	−1.14	15.65	18.35	4.72	26
Sub-lobar	Right	Insula	13	43.22	−8.81	16.79	7.47	2405
				46.8	−18.84	23.1	5.78	2405
	Left	Insula	13	−41.8	−0.21	8.95	Inf	3084
Deactivation (Baseline " >" Stimulation)								
Occipital lobe	Right	Cuneus	19	5.7	−85.41	32.32	4.14	11
	Left	Cuneus	19	−16.57	−82.09	37.66	4.37	12
Frontal lobe	Right	Precentral gyrus	4	35.51	−20.17	37.2	7.08	68
		Middle frontal gyrus	9	33.85	26.94	36.23	6.92	1078
			9	26.52	38.5	33.6	6.91	1078
			6	16.78	3.92	60.79	6.85	1078
			6	7.44	−11.29	62.79	5.25	50
			6	5.65	1.94	62.21	5.48	57
	Left	Middle frontal gyrus	9	−21.63	36.72	34.42	7.1	1388
			8	−1.39	26.6	41.01	6.42	1388
			8	−14.31	37.84	41.85	6.3	1388
			6	−1.76	−10.89	59.07	5.02	50

Table 2. Continued.

Region			BA	Talairach coordinate			Z-score	Cluster size
				X	Y	Z		
Parietal lobe	Right	Inferior parietal lobule	40	40.84	−52.92	45	Inf	414
				46.47	−50.57	39.91	7.31	414
		Inferior parietal lobule	39	42.73	−63.59	38.61	5.19	414
		Superior parietal lobule	7	24.01	−66.92	54.2	4.3	81
	Left	Inferior parietal lobule	40	−46.11	−55.85	39.65	6.1	147
		Supramarginal gyrus	40	−51.57	−53.26	32.59	5.78	147
		Inferior parietal lobule	39	−46.14	−65.17	38.76	4.98	147
		Precuneus	7	−25.88	−76.97	43.39	4.22	21
Temporal 1obe	Right	Transverse temporal gyrus	41	43.22	−27.09	11.45	5.23	117
		Middle temporal gyrus	39	52.45	−54.74	5.38	5.26	28
	Left	Superior temporal gyrus	22	−55.07	−59.13	15.76	5.19	29
Sub-lobar	Right	Insula	13	37.63	−21.82	15.46	7.13	117

Results of one-sample t-test with $P<0.001$, correcting for multiple comparisons using a false discovery rate (FDR) and the extent threshold with 10 voxels.
BA, Brodmann area.
ADC_ba, apparent diffusion coefficient (ADC) mapped with using both b0_b and b0_a for baseline scans and stimulation scans, respectively.

is enough to obtain localized neuronal signals. In general, less than b=600 s/mm^2 is enough to using in fMRI study.[1,18] Therefore, our developed sequence is good enough to use in the fMRI study. However, the b=600 s/mm^2 may be somewhat large.

2. Diffusion-based fMRI compared to BOLD fMRI

The main advantage of using diffusion-based fMRI sequence over BOLD fMRI is that the signal acquired diffusion-based fMRI is originally from the neuronal tissue rather than macrovascular structures. Most of BOLD fMRI signals are usually came from the macroscopic vascular structure in the brain. However, a diffusion-weighted spin-echo pulse sequence has a pair of diffusion gradients straddling the RF refocusing pulse. Therefore, vascular signal cannot contribute if the spins in the blood have unexpected both 90 excitation and 180 refocusing pulse. Therefore, the sources of signals from the diffusion-based fMRI are much more localized to the neuron compared to those of BOLD fMRI.

However, diffusion-based fMRI has limitation to a long acquisition time because at least four scans are required to map the isotropic ADC value for each stimulation condition. In addition, the echo time of the diffusion-based fMRI is relatively long compared to that of BOLD fMRI. This causes signal reduction in the diffusion-based fMRI. In this study, we designed the sequence to obtain the isotropic ADC value with in a single scan.[11] This is a large advantage to enhance the temporal resolution of diffusion-based fMRI study. The proposed method can be also reduced the eddy current-related artifact because of applying the bipolar gradient for each axis. The eddy current-related artifact caused by the applied diffusion gradient is usually shown in the imaging distortion.[19]

3. Limitation of this study

First, the b-value of 600 s/mm^2 was used in the diffusion-based fMRI. This value may be too large and most of neuronal activation areas may not detect with the large b-value. This causes that neuronal activation did not detect with DWI series. Therefore, in the future study, a relatively small b-value must be used to evaluate functional changes during brain stimulations. Second, TE for the diffusion-based fMRI was 70.41 ms, which is relatively long compared to that of BOLD fMRI (TE=30 ms). Therefore, to optimize the diffusion-based fMRI, the echo time should be reduced up to at least 40 ms at 3T MRI. To achieve this short echo time, the b-value should be also reduced to <100 s/mm^2 for each axis. Finally, activated and deactivated areas with ADC_ba series should be further investigated to understand the

mechanism of the diffusion-based fMRI. There were several activation areas in addition to the occipital cortex. We do not know why these areas had increased signals during the stimulation condition. Deactivation was caused by the downgrade neuronal function during the stimulation condition. Therefore, our result, which is shown in the deactivated areas during the stimulation condition, should be not artifact.

Conclusion

To evaluate the b0 dependence of the diffusion-based fMRI study, we developed a new diffusion-based fMRI sequence to generate ADC maps in a single excitation. With the new sequence, neuronal activations can be mapped with the visual stimulation condition compared to the baseline condition in the several areas in the brain. It does not need to obtain a DWI with b=0 s/mm^2 in each time point. ADC should be mapped with using both DWI and b0 images acquired with the same condition. Our proposed method is possible to be short scan time by obtaining only two DWI with b=0 s/mm^2 that one is during a baseline scan and another is during a stimulation scan. Therefore, our optimized sequence can be used in neurosciences and clinical populations.

Acknowledgements

This study was supported by a grant of the Korean Health Technology R & D Project, Ministry for Health, Welfare & Family Affairs, Republic of Korea (A092125) and the Convergence of Conventional Medicine and Traditional Korean Medicine R&D program funded by the Ministry of Health & Welfare through the Korea Health Industry Development Institute (KHIDI) (HI16C2352).

Conflicts of Interest

The authors have nothing to disclose.

Ethics Approval and Consent to Participate

The study was approved by the institutional review board (IRB approval number; KHNMC IRB 2009-056).

References

1. Darquie A, Poline JB, Poupon C, Saint-Jalmes H, Le Bihan D. Transient decrease in water diffusion observed in human occipital cortex during visual stimulation [published online ahead of print 2001/07/19]. Proc Natl Acad Sci U S A. 2001;98(16):9391-9395.
2. Roy CS, Sherrington CS. On the Regulation of the Blood-supply of the Brain [published online ahead of print 1890/01/01]. J Physiol. 1890;11(1-2):85-158.
3. Bandettini PA, Wong EC, Hinks RS, Tikofsky RS, Hyde JS. Time course EPI of human brain function during task activation [published online ahead of print 1992/06/01]. Magn Reson Med. 1992;25(2):390-397.
4. Kwong KK, Belliveau JW, Chesler DA, et al. Dynamic magnetic resonance imaging of human brain activity during primary sensory stimulation [published online ahead of print 1992/06/15]. Proc Natl Acad Sci U S A. 1992;89(12):5675-5679.
5. Ogawa S, Tank DW, Menon R, et al. Intrinsic signal changes accompanying sensory stimulation: functional brain mapping with magnetic resonance imaging [published online ahead of print 1992/07/01]. Proc Natl Acad Sci U S A. 1992;89(13):5951-5955.
6. Le Bihan D. Molecular diffusion, tissue microdynamics and microstructure [published online ahead of print 1995/11/01]. NMR Biomed. 1995;8(7-8):375-386.
7. Latour LL, Svoboda K, Mitra PP, Sotak CH. Time-dependent diffusion of water in a biological model system [published online ahead of print 1994/02/15]. Proc Natl Acad Sci U S A. 1994;91(4):1229-1233.
8. Bae MS, Jahng GH, Ryu CW, Kim EJ, Choi WS, Yang DM. Effect of intravenous gadolinium-DTPA on diffusion tensor MR imaging for the evaluation of brain tumors [published online ahead of print 2009/07/29]. Neuroradiology. 2009;51(12):793-802.
9. Jahng GH, Xu S. Local susceptibility causes diffusion alterations in patients with Alzheimer's disease and mild cognitive impairment [published online ahead of print 2012/03/15]. Brain Imaging Behav. 2012;6(3):426-436.
10. Le Bihan D, Urayama S, Aso T, Hanakawa T, Fukuyama H. Direct and fast detection of neuronal activation in

the human brain with diffusion MRI [published online ahead of print 2006/05/17]. Proc Natl Acad Sci U S A. 2006;103(21):8263-8268.
11. Song AW, Guo H, Truong TK. Single-shot ADC imaging for fMRI [published online ahead of print 2007/01/30]. Magn Reson Med. 2007;57(2):417-422.
12. Stejskal EO, Tanner JE. Spin Diffusion Measurements: Spin Echoes in the Presence of a Time-Dependent Field Gradient. J Chem Phys. 1964;42(1).
13. Lancaster JL, Tordesillas-Gutierrez D, Martinez M, et al. Bias between MNI and Talairach coordinates analyzed using the ICBM-152 brain template [published online ahead of print 2007/02/03]. Hum Brain Mapp. 2007;28(11):1194-1205.
14. Friston K, Holmes AP, Worsley KJ, Poline JB, Frith CD, Frackowiak RS. Statistical parametric maps in functional imaging: A general linear approach. Human Brain Mapping. 1995;2:189-210.
15. Talairach J, Tournoux P. Co-planar Stereotaxic Atlas of the Human Brain. Thieme. 1988.
16. Nicolas R, Gros-Dagnac H, Aubry F, Celsis P. Comparison of BOLD, diffusion-weighted fMRI and ADC-fMRI for stimulation of the primary visual system with a block paradigm. Magn Reson Imaging. 2017;39:123-131.
17. Williams RJ, Reutens DC, Hocking J. Influence of BOLD Contributions to Diffusion fMRI Activation of the Visual Cortex. Frontiers in neuroscience. 2016;10:279.
18. Zhong J, Kennan RP, Fulbright RK, Gore JC. Quantification of intravascular and extravascular contributions to BOLD effects induced by alteration in oxygenation or intravascular contrast agents [published online ahead of print 1998/10/15]. Magn Reson Med. 1998;40(4):526-536.
19. Jahng GH, Weiner MW, Schuff N. Diffusion anisotropy indexes are sensitive to selecting the EPI readout-encoding bandwidth at high-field MRI [published online ahead of print 2008/04/19]. Magn Reson Imaging. 2008;26(5):676-682.